*Fibers and Polymers 2000, Vol.1, No.1, 37-44*

# Three Dimensional FEM Simulation for Spinning of Non-circular Fibers

**Heejae Kim, Kwansoo Chung, and Jae Ryoun Youn***

*School of Materials Science and Engineering, Seoul National University, Seoul 151-742, Korea*
(Received August 11, 2000 ; Revised August 29, 2000 ; Accepted September 15, 2000)

**Abstract :** A finite element method is employed for a flow analysis of the melt spinning process of a non-circular fiber, a PET(polyethylene terephthalate) filament. The flow field is divided into two regions of die channel and spin-line. A two dimensional analysis is used for the flow within the die channel and a three dimensional analysis for the flow along the spin-line. The Newtonian fluid is assumed for the PET melt and material properties are considered to be constant except for the viscosity. Effects of gravitation, air drag force, and surface tension are neglected. Although the spin-line length is 4.5 m, only five millimeters from the spinneret are evaluated as the domain of the analysis. Isothermal and non-isothermal cases are studied for the flow within the die channel. The relationship between the mass flow rate and the pressure gradient is presented for the two cases. Three dimensional flow along the spin-line is obtained by assuming isothermal conditions. It is shown that changes in velocity and cross-sectional shape occur mostly in the region of 1mm from the die exit.

## Introduction

Melt spinning is the most common process to produce polymer fibers and a great number of researches have been devoted to it[1-7]. Mathematical models and numerical simulations have been applied to understand the process in depth. Kase and Matsuo[8] proposed an asymptotic model that gave approximate results for the circular fiber spinning with a minimum period of calculation time. This method, utilizing thin filament equation, assumes that variations in the radial direction are negligible because the radius of the filament is so small compared with the spin-line length. They integrated a set of equations over the cross-section of the filament in which parameters have no dependence on radial direction. With some empirical relations for physical properties and heat transfer coefficients, they obtained numerical simulation results for the Newtonian fluid. Other constitutive equations were also used for modeling of the melt spinning. Matovich and Pearson[9] used the second order Coleman and Noll fluids, and Han and Segal[10] applied the three constant Oldroyd model to the problem of isothermal spinning. Denn *et al.*[11,12] employed the White-Metzner model and the Phan Thien and Tanner model in an isothermal case.

Studies on temperature profiles along the spin-line have been another topic in the analysis of the melt spinning process. Barnett[13] considered free and forced convection boundary conditions and obtained a temperature distribution inside the fiber. Copley and Chamberlain [14] employed radiative and convective heat transfer conditions and showed an axial temperature distribution. Chung and Iyer[15] investigated a melt spinning process considering the radial conduction and radiation effects.

Besides the asymptotic analysis, numerical methods such as the finite element method and finite difference method have been also applied[16,17]. However, the finite element method has seldom been applied to the entire domain of the spinning system because the spin-line has a large length to diameter(L/D) ratio. Thus the use of the finite element method was restricted to the study of die swell, the initial profile development over the limited region near the spinneret orifice. There have been attempts to predict the internal thermal stress from the temperature distribution[15,18-23,55-60].

In the high speed spinning of PET, the effect of air drag cannot be neglected. Matui[24] investigated the effect of the air drag on a continuous filament having constant diameter and velocity. Kwon and Prevosek[25] measured the magnitude of air drag and obtained an air velocity profile around the filament in the surroundings of stagnant air. Gould and Smith[26] studied the effect of geometry while Bos[54] investigated the mechanism of air drag using the concept of the sublayer of turbulent air flow. Molecular orientation and crystallization of polymers are gaining attention in the high speed spinning process. In addition, skin-core formation, necking phenomena, and flow resonance problems are also becoming more important[27-40].

Control of the cross-sectional shape is also widely studied and various methods are already used to obtain noncircular cross-sectional fibers. Dies with noncircular shapes can be used. By gathering filaments from many orifices together, noncircular fibers can also be produced. Elimination of one component or division into each component out of bicomponent fibers will produce non-circular fibers. A method of pressing neighboring circular fibers closely together above softening temperature is also employed[42-44]. Other methods were also devel-

*To whom correspondence should be addressed:
jaeryoun@gong.snu.ac.kr

oped in addition to those mentioned above. Among them, the method using a noncircular orifice is most common due to low production cost and good spinnability.

However, unlike the amount of literature dealing with the melt spinning process of circular fibers, many theoretical studies on the noncircular filament spinning have not been reported. Usually it is more difficult to attain stability for the noncircular filament spinning due to asymmetry of the die. Since the noncircular fiber has larger specific surface area than the circular one, solidification will be faster due to higher rate of heat and mass transfer. This leads to a shorter deformation length, larger velocity gradient, and higher degree of molecular orientation. One of the main problems is that the cross-section of the as-spun fiber is generally different in shape from that of the spinneret orifice[41,45,46].

Many studies on die swell have been performed. Han *et al.*[47], and Huang and White[48] obtained experimental results on the die swell of noncircular fibers produced without a draw-down. According to Ziabicki[1], the cross-sectional shape of the filament within the spin-line region would be intermediate between the shapes of die and the as-spun fiber. Han *et al.*[49] investigated the effect of air cooling distance and draw-down ratio on molecular orientation for noncircular fiber spinning. Noh[50], and Park and Kim[51] studied the rectangular fiber spinning theoretically and experimentally. Jung[52] reported the experimental results on the shape change of the trilobal fibers.

In this work, dimensional change during melt spinning of the trilobal PET filament is analyzed by an Eulerian FEM (finite element method). It is assumed that the major change in the cross-sectional shape of the filament occurs only during die swell after which the cross-sectional area does not change. Therefore, the limited region near the spinneret orifice is the focus of this work.

Numerical simulation results are compared with the experimental data that are supplied by SK Chemicals. All the material properties are set to be the same as those of PET used in the industry. The shape of the die channel and the cross-sectional shape of the as-spun filament produced are shown in Figure 1.

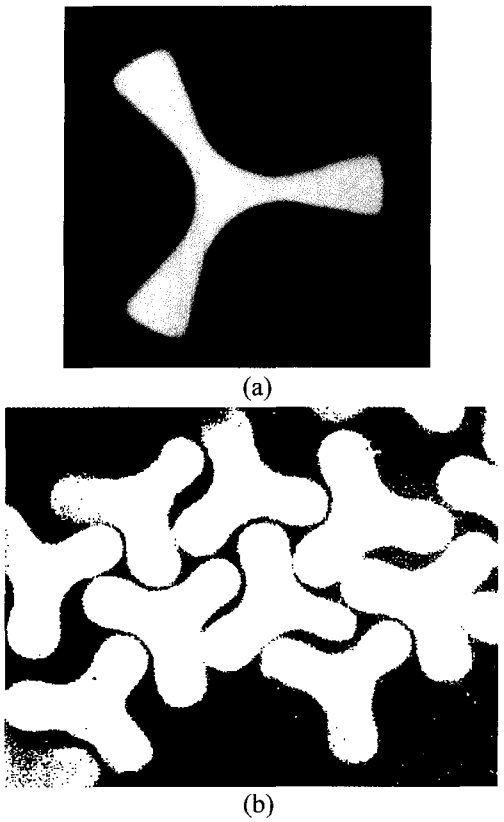


**Figure 1.** Cross-sectional shapes of the spinneret and fibers; (a) trilobal shape of the die channel, (b) cross-sectional shape of the as-spun filament.

## Formulation and Numerical Method

In order to investigate the dimensional variation of the noncircular fiber along the spin-line, the application of the 3-D analysis is quite essential because the cross-sectional geometry may be arbitrary. In this work, the flow behavior within the die channel and along the spin-line is considered separately to reduce the degree of freedom and only the latter is analyzed three dimensionally.

It is well known that PET shows Newtonian behavior over the broad range of shear rate. Although the flow that occurs during the spinning process is not entirely shearing, the Newtonian viscosity model is assumed for PET in this study. The Newtonian viscosity is given as a function of temperature only. And the thermal conductivity of PET is assumed to be constant[53,61]. Since only a few millimeters of spin-line from the spinneret is the domain of interest in this study, effects of gravity, surface tension,

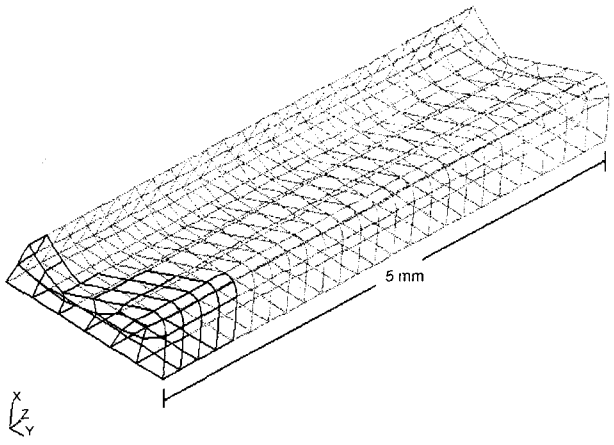


**Figure 2.** Initial meshes for the 3-D analysis of the spin-line.

and air drag are neglected throughout this work. Initial mesh employed for three dimensional analysis of the spin-line is presented in Figure 2.

**Flow within the Die Channel**

Assuming that the flow within the die channel is steady and homogenous, two dimensional analysis is used for prediction of pressure and velocity fields. The cross-sectional area is discretized by 15 finite elements (Figure 3). From the above assumption, velocity components are given as below

$$u = v = 0,\ w = w(x, y) \tag{1}$$

and the continuity equation for incompressibility is satisfied spontaneously. Here, $u$, $v$, and w are velocity components in $x$, $y$, and $z$ directions, respectively.

Governing equations are shown below:

$$-\frac{\partial p}{\partial z} + \frac{\partial}{\partial x}\left(\eta\frac{\partial w}{\partial x}\right) + \frac{\partial}{\partial y}\left(\eta\frac{\partial w}{\partial y}\right) = 0 \tag{2}$$

$$k\left(\frac{\partial^2 T}{\partial x^2} + \frac{\partial^2 T}{\partial y^2}\right) + \eta\left[\left(\frac{\partial w}{\partial x}\right)^2 + \left(\frac{\partial w}{\partial y}\right)^2\right] = 0 \tag{3}$$

where $p$ denotes hydraulic pressure and $T$ temperature in Celsius. The thermal conductivity and the viscosity are given as

$$k = 37.5 \times 10^{-3}\ (\mathrm{W/m \cdot K}) \tag{4}$$

$$\eta(T) = 9.76 \times 10^{-3} \times (I.V.)^{5.29} \times \exp\left[\frac{6923.7}{T + 273}\right]\ (Pa \cdot s) \tag{5}$$

where I.V. is the intrinsic viscosity of PET.

Along the boundary of the die wall, non-slip condition and the essential boundary condition for die wall temperature are applied. Symmetry condition is given to the rest of the boundary. The 8 noded quadrilateral finite elements are used for two dimensional simulation. The field variables of $w$ and $T$ are approximated with the isoparametn interpolation function.

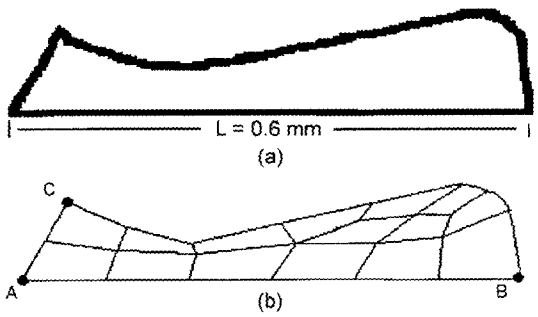


**gure 3.** Numerical analysis domain and the finite element shes; (a) domain for 2-D analysis within the die (1/6 of the ole domain), (b) FEM elements.

**Flow along the Spin-Line**

Spin-line of 5 mm from the die exit is selected as the domain of analysis because a large amount of time and computer memory are required to consider the whole length of spin-line due to the high aspect ratio of the filament. However, it is generally known that the velocity profile of the flow will become the plug flow before the extrudate travels the distance two or three times the spinneret diameter in the downstream direction. The domain of analysis is evenly divided by finite elements whose length is 0.1 mm in the $z$ direction. To simplify the problem, an isothermal case is considered and the shape of the free surface is obtained by using the z-directional velocity component. Positions of surface nodes are determined by satisfying the continuity condition within each element. If the variables for pressure and velocity converge to some extent, the shape of the free surface is recalculated and updated, and the nodes of inner domain are regenerated. The overall procedure is shown schematically in Figure 4.

Governing equations for the steady incompressible flow are given below.

i. Continuity Equation

$$\frac{\partial u}{\partial x} + \frac{\partial v}{\partial y} + \frac{\partial w}{\partial z} = 0 \tag{6}$$

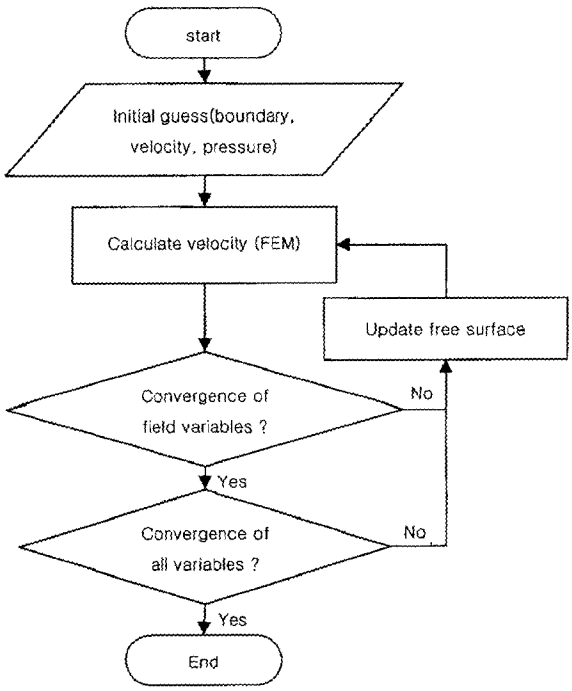


**Figure 4.** Flow chart for the simulation of the flow field along the spin-line.

ii. Momentum Equations

$$\rho\left(u\frac{\partial u}{\partial x}+v\frac{\partial u}{\partial y}+w\frac{\partial u}{\partial z}\right)=-\frac{\partial p}{\partial x}+\left(\frac{\partial \tau_{xx}}{\partial x}+\frac{\partial \tau_{yx}}{\partial y}+\frac{\partial \tau_{zx}}{\partial z}\right) \quad (7)$$

$$\rho\left(u\frac{\partial v}{\partial x}+v\frac{\partial v}{\partial y}+w\frac{\partial v}{\partial z}\right)=-\frac{\partial p}{\partial y}+\left(\frac{\partial \tau_{xy}}{\partial x}+\frac{\partial \tau_{yy}}{\partial y}+\frac{\partial \tau_{zy}}{\partial z}\right) \quad (8)$$

$$\rho\left(u\frac{\partial w}{\partial x}+v\frac{\partial w}{\partial y}+w\frac{\partial w}{\partial z}\right)=-\frac{\partial p}{\partial z}+\left(\frac{\partial \tau_{xz}}{\partial x}+\frac{\partial \tau_{yz}}{\partial y}+\frac{\partial \tau_{zz}}{\partial z}\right) \quad (9)$$

where $\rho$ is the density of PET and $\tau_{ij}$ denotes the component of deviatoric stress tensor.

Traction free conditions are assumed at the boundary of free surface. The velocity profile obtained from the two dimensional simulation for the flow within the die channel is given as an essential condition at the die exit. A plug flow profile(0.050754 m/s) is assumed at the last surface in the downstream direction(z = 5 mm). Symmetry condition is used for the rest of the boundary.

20 noded three dimensional brick elements, which is an extension of the two dimensional 8 noded quadrilateral element to the three dimensional case, are used. Two different interpolation functions are used for determining pressure and velocity fields, respectively. Pressure distribution is interpolated by a linear function and velocity by a quadratic function.

## Results and Discussion

### Material Properties and Processing Conditions

Experiments were conducted in an industry laboratory and the final cross-sectional shape of the fiber was observed. Material data and the experimental conditions were supplied by the SK Chemicals as given in Table 1.

### Flow within the Die Channel

In addition to the experimental conditions, some other assumptions are made for the numerical analysis. In order to understand the effect of the pressure gradient on the velocity profile and mass flow rate, calculations were carried out for various values of the pressure gradient, both for isothermal and non-isothermal cases. For given pressure gradients in the orifice, velocity profiles differ in the isothermal and non-isothermal cases. Each of the two cases gives different mass flow rate at the same pressure gradient and the difference in mass flow rate becomes larger as the pressure gradient increases. Comparative

**Table 1.** Material properties and process conditions

| | |
|---|---|
| · Intrinsic Viscosity of PET | 0.63 |
| · Tg of PET | 75°C |
| · Tm of PET | 258°C |
| · Density of PET | 1.38 (solid)/1.20 (melt) g/cm$^3$ |
| · Spinning Temperature | 290°C |
| · Air Temperature | 25°C |
| · Relative Humidity of Air | 65% |
| · Mass Throughput | 33.3 g/min ( per 24 holes) |
| · Take-up Speed | 1300 m/min (21.7 m/s) |
| · Length of the Spin-line | 4.5 m |

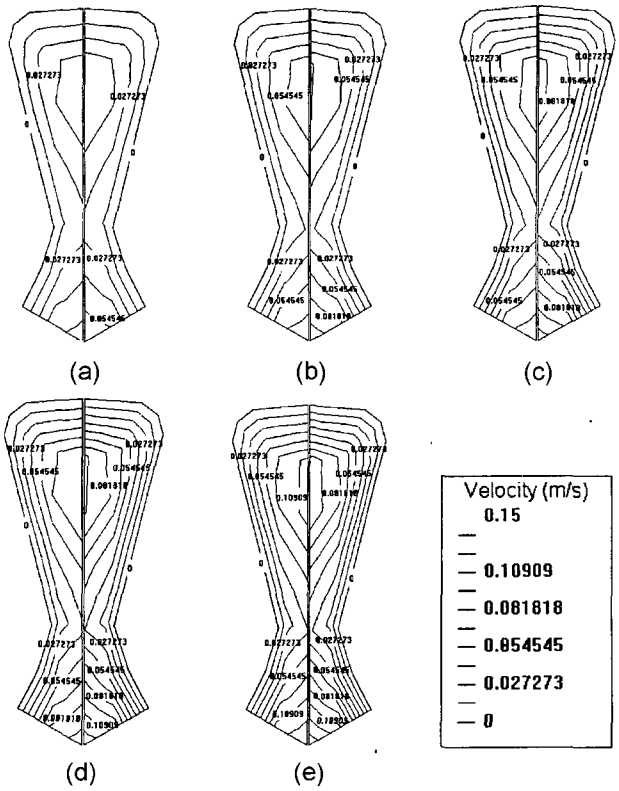


**Figure 5.** Velocity contours within the die channel in the isothermal and non-isothermal cases for the pressure gradients of (a) 2.1, (b) 2.7, (c) 3.2, (d) 3.5, (e) 3.6×10$^9$ Pa/m (left - isothermal).

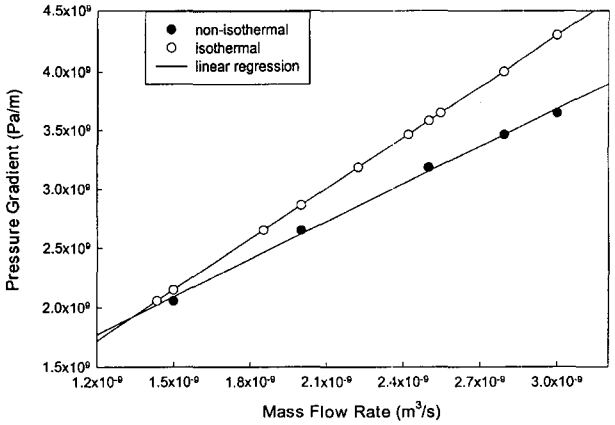


**Figure 6.** Relationship between the pressure gradient and the mass flow rate in the die channel.

views of velocity profiles for isothermal and non-isothermal cases are provided in Figure 5 and the relationship between the pressure gradient and the mass flow rate is shown in Figure 6. Compared with the isothermal cases, numerical results for non-isothermal cases slightly deviate from the linear regression line as shown in Figure 6. Even though the trend cannot be seen obviously in the graph, the slope of the curve for the non-isothermal case decreases with the increase in the mass flow rate. Considering the viscous heat dissipation, the slope must be lower

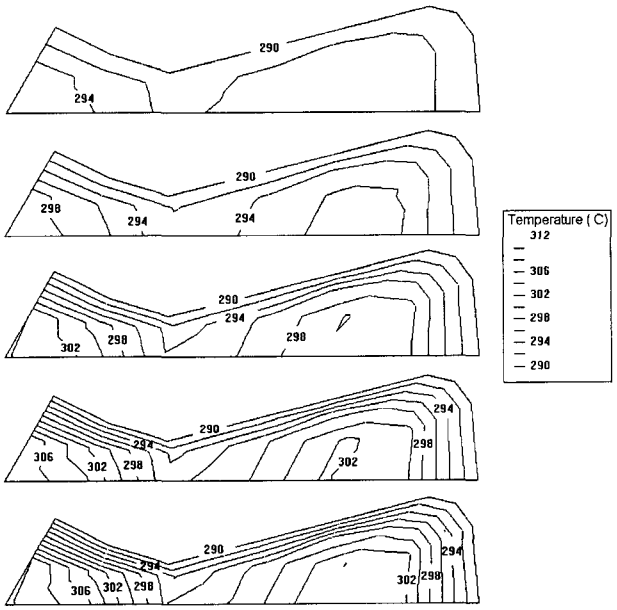


**Figure 7.** Temperature contours within the die channel (from the top, mass flow rates of 9, 12, 15, 16.7, and 18 $m^3/s$).

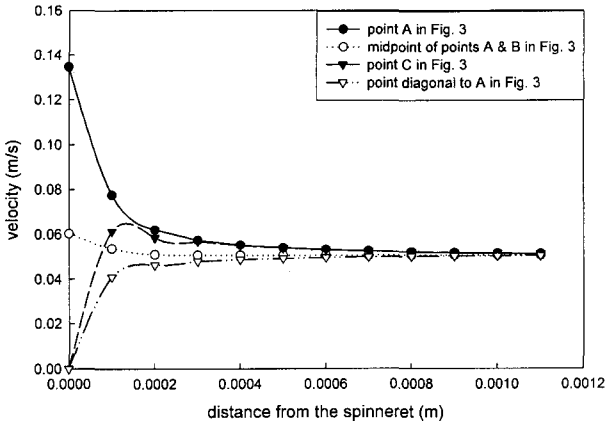


**Figure 8.** z-directional velocity variation along the spin-line at four different locations.

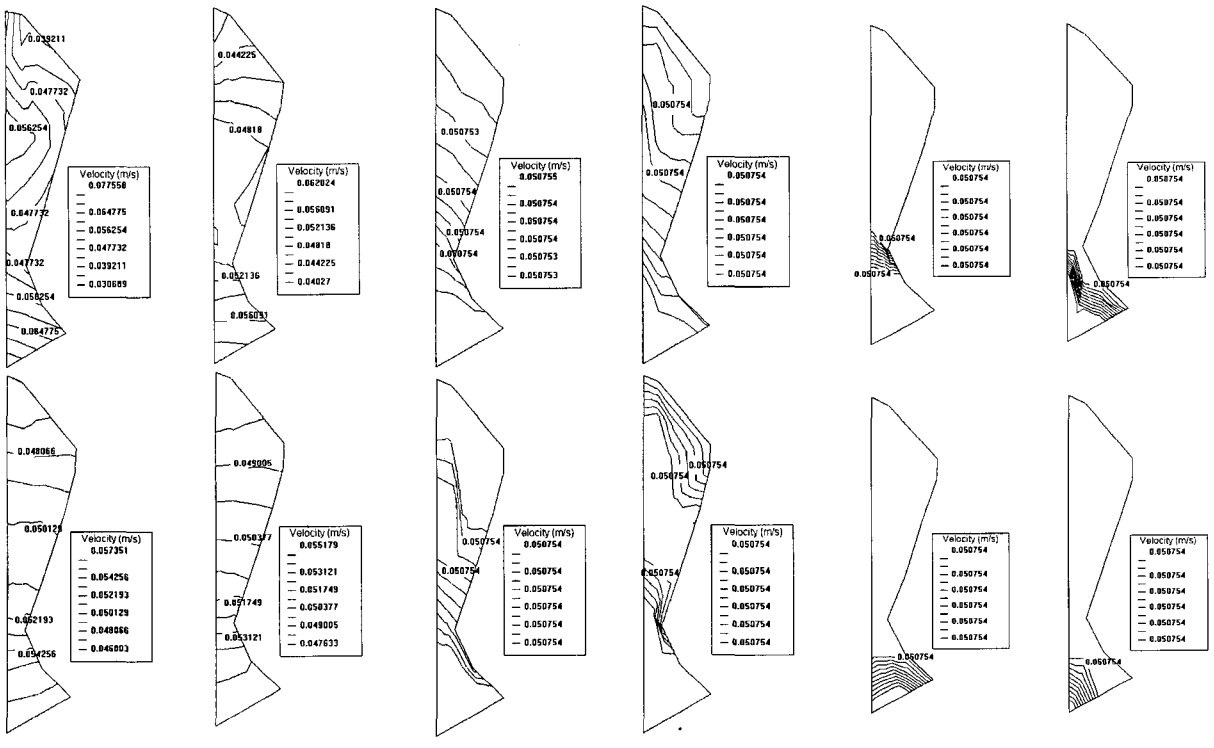


**Figure 9.** z-directional velocity contours at different distances from the spinneret; (a) 0.1/0.2/0.3/0.4, (b) 3.0/3.5/3.6/3.8, (c) 3.9/41/4.2/4.3 mm.

at the larger mass flow rate. Since the analysis is conducted over a sixth of the whole cross-sectional area of the orifice, the mass flow rate through the entire die channel is six times the flow rate presented in the graph.

The temperature distributions are shown in Figure 7 for the non-isothermal cases. The larger the pressure gradient is, the larger the high temperature region. Because the temperature increases by viscous heat dissipation, the temperature contour lines are similar to those of velocity contour lines.

**Flow along the Spin-line**

To achieve the convergence during the numerical analysis, the z-directional velocity component, $w$, is obtained first and the rest of variables are calculated. The variation of $w$ along the spin-line is shown in Figure 8. At the center where $w$ has the largest value, the velocity at the exit of the die channel ($z = 0$) approaches the value of the plug flow rapidly. On the contrary, at the free surface where $w$ is zero at the exit of the die channel, the velocity increases to the value of the velocity of plug flow. But there are various saturation rates to the velocity of plug flow along the boundary of the free surface. A small overshoot of velocity occurs at points on the free surface near the center while the velocity converges monotonously to the plug flow velocity at points far from the center. These tendencies can be explained by the fact that the velocity gradient in the direction of x-axis is larger due to short distance and larger viscous force acts in this direction. Since the effect of elongation is weak in the domain of analysis, the changes in velocity are mainly due to viscous force and the curves shown in Figure 8 do not vary exponentially.

In Figure 9, it can be seen that velocity contour lines are aligned along the direction of the x-axis after some adjustment near the spinneret. As the fiber flows to the downstream, the contour lines become parallel to the free surface. But it should be noted that the scales are different for each contour plot and the gap between contour lines becomes narrower as the distance from the die exit increases. It can also be known that major changes in the cross-sectional shape occur over the short distance from the spinneret. Gradual changes of the finite element meshes in the cross-sectional area are shown in Figure 10.

Since it is somewhat difficult to compare the size of each cross-section, die swell ratios are plotted along the spin-line in Figure 11. It is seen that swelling is not isotropic and bulging in the x-axis direction is larger. Compared with the experimental results, however, the predicted swelling in the x direction is not large enough.

After proper manipulation, shape of the filament is predicted and depicted in Figure 12 together with cross-sectional shape of the spun fiber obtained by the experiment. As shown in the figure, there is a substantial difference between the experimental and simulation results. It is well known that the effect of surface tension is negligible near the spinneret due to large rheological force. However, in

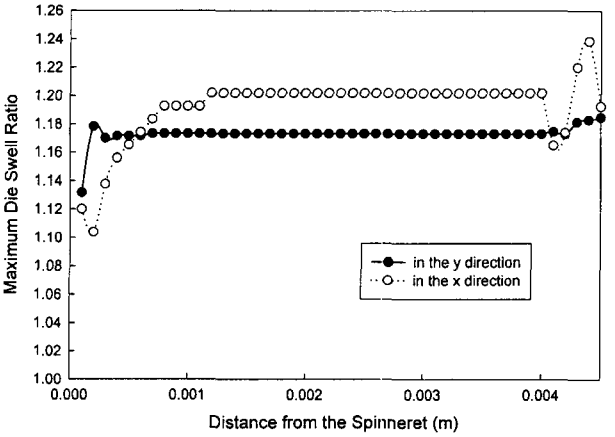


**Figure 11.** Die swell ratio along the spin-line.

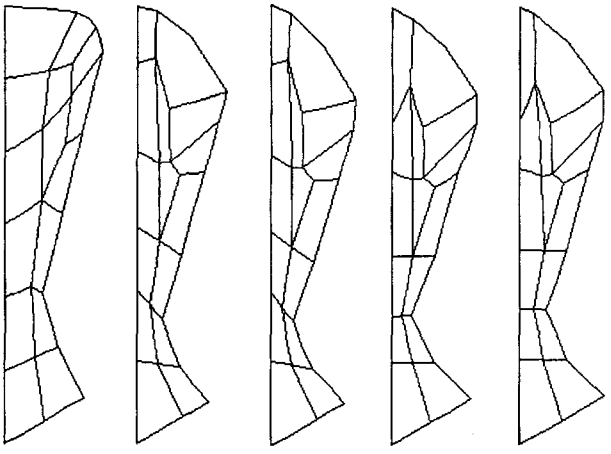

**Figure 10.** Changes in cross-sectional shape along the spin-line (from the left, z = 0.0/0.1/0.2/4.2/4.8 mm).

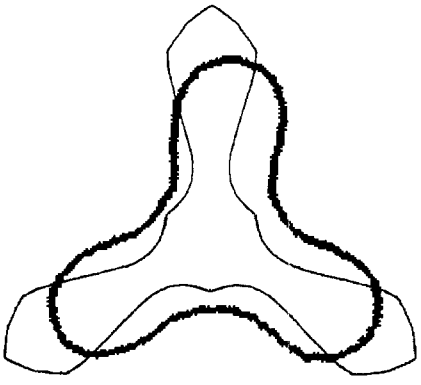

**Figure 12.** Comparison of calculated and experimental cross-sectional shapes (thick line : experiment).

non-circular fiber spinning, surface tension can be a key factor that contributes to the shape change. Consideration of the surface tension in the analysis would result in a smaller aspect ratio of lobes. Because the concave portions predicted by the numerical computation do not bulge enough, the cross-sectional shape obtained by the simulation does not form smooth curves. Application of the surface tension in computing the shape of free surface may improve the calculation results.

## Conclusions

As the result of numerical analysis on non-circular fiber spinning, velocity profiles within the spinneret orifice and along the spin-line are obtained. In the die channel, a larger pressure gradient is needed to achieve the same mass flow rate in the isothermal case than in the non-isothermal case. The pressure difference increases with the mass flow rate due to higher viscous friction. Analysis for the spin-line is more complex and the isothermal case is considered for the numerical simulation. Variations in the velocity distribution and the cross-sectional shape take place mainly in a local region, several tenths of millimeters from the spinneret, and it is a small distance compared with the orifice radius, 0.6 mm. A plug flow occurs soon after the melt is extruded from the spinneret orifice. Die swell ratio in x-direction is larger than that in y-direction. However, the die swell in the x-axis direction is small compared with the experimental results.

## Acknowledgement

This work has been supported by the Korea Science and Engneering Foundation (KOSEF). The authors are grateful for the support.

## References

1. A. Ziabicki, "Fundamentals of Fiber Formation", Wiley Interscience, London, 1976.
2. D. G. Baird and D. I. Collias, "Polymer Processing", Butterworth-Heinemann, Boston, 1995.
3. A. Ziabicki and H. Kawai, "High-speed Fiber Spinning", Wiley Interscience, New York, 1985.
4. S. Middleman, "Fundamentals of Polymer Processing", McGraw-Hill Inc., New York, 1977.
5. R. W. Moncrieff, "Man-made Fibers", Butterworth, London, 1975.
6. Z. Tadmor, C. G. Gogos, "Principles of Polymer Processing", Wiley Interscience, New York, 1979.
7. T. Nakajima, "Advanced Fiber Spinning Technology", Woodhead, Cambridge, 1994.
8. S. Kase and T. Matsuo, *J. Polym. Sci.*, **3**, 2541 (1965).
9. M. A. Matovich and J. R. A. Pearson, *I&EC. Fund.*, **8-3**, 512 (1969).
10. C. D. Han and L. Segal, *J. Appl. Polym. Sci.*, **14**, 2973 (1970).
11. M. M. Denn, C. J. S. Petrie, and P. Avenas, *AIChE. J.*, **21**(4), 791 (1975).
12. D. K. Gagon and M. M. Denn, *Polym. Eng. & Sci.*, **21**, 844 (1981).
13. T. R. Barnett, *Appl. Polym. Sym.*, **6**, 51 (1967).
14. M. Copley and N. H. Chamberlain, *Appl. Polym. Sym.*, **6**, 27 (1967).
15. B. T. F. Chung and V. Iyer, *J. Appl. Polym. Sci.*, **44**, 663 (1992).
16. J. R. Fisher, M. M. Denn, and R. I. Tanner, *Ind. Eng. Chem. Fundam.*, **19**, 195 (1980).
17. J. R. A. Pearson and S. M. Richardson, *"Computational Analysis of Polymer Processing"*, Applied Science Publishers, London, 1983.
18. M. J. Crochet and R. Keunings, *J. Non-Newt. Fluid Mech.*, **7**, 199 (1980).
19. E. Mitsoulis and F. L. Heng, *Rheol. Acta*, **26**, 414 (1987).
20. M. J. Crochet and R. Keunings, *J. Non-Newt. Fluid Mech.*, **10**, 85 (1982).
21. R. E. Nickell, R. I. Tanner, and B. Caswell, *J. Fluid Mech.*, **65**, 189 (1974).
22. W. P. Bell and D. D. Edie, *J. Appl. Polym. Sci.*, **33**, 1073 (1987).
23. K. W. Hutchenson, D. D. Edie, and D. M. Riggs, *J. Appl. Polym. Sci.*. **29**, 3621 (1984).
24. M. Matui, *Trans. Soc. Rheol.*, **20:3**, 465 (1976).
25. Y. D. Kwon and D. C. Prevosek, *J. Appl. Polym. Sci.*, **23**, 3105 (1979).
26. J. Gould and F. S. Smith, *J. Text. Inst.*, **No. 1**, 38 (1980).
27. A. Dutta, *Tex. Res. J.*, **57**, 13 (1987).
28. A. Dutta, *Tex. Res. J.*, **59**, 411 (1989).
29. A. Dutta, *Polym. Eng. & Sci.*, **27**, 1050 (1987).
30. A. Dutta, and V. M. Nadkarni, *Tex. Res. J.*, **54**, 35 (1984).
31. A. V. Shenoy and V. M. Nadkarni, *Tex. Res. J.*, **54**, 778 (1984).
32. C. Jinan, T. Kikutani, A. Takaku, and J. Shimizu, *J. Appl. Polym. Sci.*, **37**, 2683 (1989).
33. R. M. Patel, J. H. Bheda, and J. E. Spruiell, *J. Appl. Polym. Sci.*, **42**, 1671 (1991).
34. C. T. Kiang and J. A. Cuculo, *J. Appl. Polym. Sci.*, **46**, 55 (1992).
35. C. T. Kiang and J. A. Cuculo, *J. Appl. Polym. Sci.*, **46**, 67 (1992).
36. J. F. Hotter, J. A. Cuculo, and P. A. Tucker, *J. Appl. Polym. Sci.*, **43**, 1511 (1991).
37. J. S. Denton, J. A. Cuculo, and P. A. Tucker, *J. Appl. Polym. Sci.*, **57**, 939 (1995).
38. Y. C. Bhuvanesh and V. B. Gupta, *J. Appl. Polym. Sci.*, **58**, 663 (1991).

39. K. F. Zieminski and J. E. Spruiell, *J. Appl. Polym. Sci.*, **35**, 2223 (1988).
40. C. Y. Lin, P. A. Tucker, and J. A. Cuculo, *J. Appl. Polym. Sci.*, **46**, 531 (1992).
41. T. Hongu and G. O. Philips, "New Fibers", New York, Ellis Horwood, 1990.
42. M. Lewin and J. Preston, "Handbook of Fiber Science & Technology: Vol. High Technology Fibers part D", Marcel Dekker Inc., New York, 1983.
43. C. W. Park, *AIChE. J.*, **36**, 197 (1990).
44. W. S. Lee and C. W. Park, *J. Appl. Mech.*, **36**, 511 (1990).
45. M. A. Huneault, P. G. Lafleur, and P. J. Carreau, *Polym. Eng. & Sci.*, **30**, 1544 (1990).
46. R. M. Griffith and J. T. Tsai, *Polym. Eng. & Sci.*, **20**, 1811 (1980).
47. C. D. Han, "Rheology in Polymer Processing", Academic Press, New York, 1976.
48. D. C. Huang and J. L. White, *Polym. Eng. Sci.*, **19**, 609 (1979).
49. C. D. Han, R. R. Lamonte, and L. H. Drexler, *J. Appl. Polym. Sci.*, **17**, 1165 (1973).
50. Y. W. Noh, "Studies on the Melt Spinning of Rectangular PET Fibers", Ph.D. Dissertation, SNU, 1996.
51. J. W. Park and H. Y. Kim, *J. Kor. Fiber Soc.*, **34**, 119 (1997).
52. I. Jung, M. S. Thesis, SNU, 1999.
53. T. H. Oh, P. S. Lee, S. Y. Kim, and H. J. Shim, *Tex. Res. J.*, **68**, 449 (1998).
54. C. Bos, *Int. J. Heat Mass Transfer*, **31(1)**, 167 (1988).
55. N. Phan-Thien, *J. Non-Newt. Fluid Mech.*, **26**, 327 (1988).
56. B. J. Yarusso, *J. Non-Newt. Fluid Mech.*, **40**, 103 (1991).
57. A. N. Hrymak, and J. Vlachopoulos, *Rheol. Acta*, **28**, 121 (1989).
58. A. Karaginnis, A. N. Hrymak, and J. Vlachopoulos, *AIChE. J.*, **34**, 2088 (1988).
59. A. A. Hamza and H. I. A. El-Kader, *Tex. Res. J.*, **53**, 205 (1983).
60. R. Keunings, M. J. Crochet, and M. M. Denn, *Ind. Eng. Chem. Fundam.*, **22**, 347 (1983).